Geophysical Prospecting, 1996, 44, 687–717

A physical model for shear-wave velocity prediction[1]

Shiyu Xu[2] and Roy E. White[2]

Abstract

The clay–sand mixture model of Xu and White is shown to simulate observed relationships between S-wave velocity (or transit time), porosity and clay content. In general, neither S-wave velocity nor S-wave transit time is a linear function of porosity and clay content. For practical purposes, clay content is approximated by shale volume in well-log applications. In principle, the model can predict S-wave velocity from lithology and any pair of P-wave velocity, porosity and shale volume. Although the predictions should be the same if all measurements are error free, comparison of predictions with laboratory and logging measurements show that predictions using P-wave velocity are the most reliable. The robust relationship between S- and P-wave velocities is due to the fact that both are similarly affected by porosity, clay content and lithology. Moreover, errors in the measured P-wave velocity are normally smaller than those in porosity and shale volume, both of which are subject to errors introduced by imperfect models and imperfect parameters when estimated from logs.

Because the model evaluates the bulk and shear moduli of the dry rock frame by a combination of Kuster and Toksöz' theory and differential effective medium theory, using pore aspect ratios to characterize the compliances of the sand and clay components, the relationship between P- and S-wave velocities is explicit and consistent. Consequently the model sidesteps problems and assumptions that arise from the lack of knowledge of these moduli when applying Gassmann's theory to this relationship, making it a very flexible tool for investigating how the v_P–v_S relationship is affected by lithology, porosity, clay content and water saturation. Numerical results from the model are confirmed by laboratory and logging data and demonstrate, for example, how the presence of gas has a more pronounced effect on P-wave velocity in shaly sands than in less compliant cleaner sandstones.

Introduction

Shear-wave velocity logs are essential to the interpretation of amplitude-versus-offset analyses and multicomponent seismic and VSP data. Although the logging

[1] Paper presented at the 56th EAEG meeting, June 1994, Vienna, Austria. Received October 1994, revision accepted November 1995.

[2] Research School of Geological and Geophysical Sciences, Birkbeck and University Colleges, University of London, Malet Street, London WC1E 7HX, UK.

industry now offers a number of S-wave velocity tools, they have been run in relatively few wells and are still not used routinely. There is therefore a need to predict S-wave velocities from other logs whenever measured S-wave velocity logs are unavailable. Even when an S-wave log has been run, comparison with its prediction from other logs can be a useful quality control. Prediction can be used to fill gaps in S-wave logs run with, say, monopole sources or to enhance the resolution of logs from long spacing tools.

A number of empirical laws have been published. These can be divided into four categories:

1. v_S (S-wave velocity) is a linear function of v_P (P-wave velocity) as in Castagna's mudrock line (Castagna, Batzle and Eastwood 1985);
2. v_S is a linear function of porosity (ϕ) and clay content V_{sh} (Tosaya 1982; Castagna *et al.* 1985; Han, Nur and Morgan 1986);
3. S-wave transit time T^S is a linear function of porosity and clay content (e.g. Castagna *et al.* 1985);
4. shear modulus is a linear function of porosity (e.g. Blangy and Nur 1992).

In general empirical models are simple and straightforward. Some empirical relationships, like the time-average equation and Archie's law, are still widely used in the oil industry today.

The disadvantages of empirical relationships are:

1. they tell us very little about the physical mechanisms of rock properties;
2. a large quantity of data and detailed analysis are needed to establish a reliable relation;
3. their conditions of validity may not be well defined.

It is therefore useful to have a physical model that provides some understanding of S-wave behaviour. If an S-wave sonic log is available, such a model may help geophysicists, log analysts or petrophysicists interpret the measurements.

Greenberg and Castagna (1992) developed a semiphysical model in order to predict S-wave velocity in porous rocks. The authors employed an empirical relationship to relate S-wave velocity to compressional velocity in fully brine-saturated rocks. Wood's (1941) suspension model was used to average the bulk modulus of pore fluids if partially saturated, and the Voigt–Reuss–Hill (Wang and Nur 1992) equation was used to estimate mixed grain incompressibility. Applications of the Greenberg and Castagna (1992) model to both laboratory measurements and logging data show that S-wave velocity can be estimated with a precision of better than 7%. The success of the model was attributed to the robust relationship between P-wave and S-wave velocities but there was no physical model of the relationship itself.

Xu and White (1995a) proposed a clay–sand mixture model based on the Kuster and Toksöz (1974), Gassmann (1951) and differential effective medium (DEM) theories, which related P-wave velocity in sand–shale systems to porosity and clay content. The applicability of the model was confirmed by comparing its predictions with laboratory measurements and sonic logs recorded over depth intervals where

formations varied from unconsolidated and uncemented to consolidated sand–shale sequences (Xu and White 1995a).

This paper demonstrates that the clay–sand mixture model can predict S-wave velocity in siliciclastic rocks as well as or better than *P*-wave velocity. We begin with a review of the model and then demonstrate how the model simulates observed relationships between S-wave velocity and porosity and clay content. The model thus provides a basis for predicting S-wave velocity from rock parameters or from other logs. It is applied to the laboratory measurements of Rafavich, Kendall and Todd (1984) and Han *et al.* (1986) and to two sets of S-wave and other log data provided by BP. Finally, the effects of clays and water saturation on the v_P/v_S ratio are investigated.

The clay–sand mixture model

The clay–sand mixture model (Xu and White 1995a) is a physical model for velocities in siliciclastic rocks developed from the Kuster–Toksöz (1974), DEM (Bruner 1976; Cheng and Toksöz 1979) and Gassmann (1951) theories. The model has two key features. The first is that it characterizes the compliances of the sand and clay mineral fractions of the rock by assigning to them separate pore spaces having different effective pore aspect ratios (ratios of short semi-axis to long semi-axis). The second key feature is the use of Kuster and Toksöz (1974) and DEM theories to compute the elastic moduli of the dry frame. Given the dry frame moduli, application of Gassmann's (1951) equations then gives the low-frequency velocity in the fluid-saturated rock.

The inputs required by the model comprise the densities and elastic moduli of the sand grains, clay particles and the pore fluid, the porosity and clay content of the rock frame, and two aspect ratios, one (α_s) for pores associated with sand grains and one (α_c) for pores associated with clay minerals (including bound water). Shale volume replaces clay content in well-log applications. Details of how these parameters are determined is included with the discussion of practical examples but, apart from the aspect ratios, they come from tabulated values and log or laboratory measurements. The aspect ratios cannot be measured directly and their estimation relies on a best fit to log or laboratory observations. All results to date show that α_s is close to 0.1 and α_c is of the order of 0.03. Xu and White (1995a, Fig. 1) give a flow chart showing how P-wave and S-wave transit times (strictly slownesses, reciprocals of velocities) are constructed from these inputs.

The use of two aspect ratios to describe the hypothesized different pore spaces associated with the sand and clay mineral fractions of the rock is obviously a gross simplification. A model with two aspect-ratio distributions may be more plausible but the need to specify the parameters of such distributions makes this option utterly impractical. In fact a single aspect ratio can simulate the elastic response of a uniform distribution of pores rather well (M. Sams, pers. comm.). As logs give no information on the pore volumes related to sand grains and to clays, we compute these on the

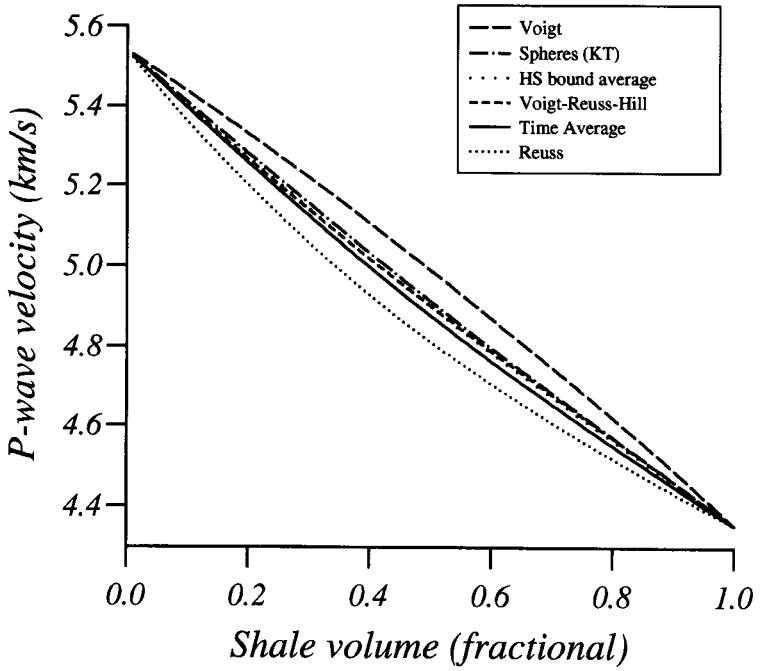

Figure 1. Comparison of P-wave velocities of the sand grain and clay particle mixture estimated using various averaging schemes. P-wave, S-wave velocities and density of the sand grain used in this simulation are 5.86 km/s, 3.91 km/s and 2650 kg/m^3, and those for clay particles are 4.45 km/s, 2.54 km/s and 2600 kg/m^3.

assumption that, to a first-order approximation, they are proportional to sand-grain volume and clay content (see Appendix; the fractional sand volume is obtained by subtracting the total porosity and fractional clay volume from one).

In order to apply Kuster and Toksöz' (1974) theory to computation of the elastic properties of the dry frame, we need the bulk and shear moduli of the mixture of sand grains and clay minerals. There are several averaging schemes available in the literature which can be used to approximate the effective elastic constants of the grain mixtures. Figure 1 shows numerical results from some commonly used schemes described by Wang and Nur (1992). As this figure shows, the Voigt scheme provides an upper bound while the Reuss scheme provides a lower bound; the Kuster and Toksöz (1974) formulation for spheres is nearly identical to the Hashin–Shtrikman upper bound, the time-average approximation is very close to the Hashin–Shtrikman lower bound (the bounds are not plotted to avoid crowding the diagram further) while the Voigt–Reuss–Hill average scheme and the Hashin–Shtrikman bound average fall between the time-average and the Kuster and Toksöz (1974) approximation for spheres.

Apart from the Voigt and Reuss schemes, there is little to choose between the proposed schemes. The reason for this lies in the low velocity contrast between

different grain minerals. We used time-average equations to compute P- and S-wave transit times of the grain mixture because we believe they provide a simple and close approximation to the low-frequency conditions that mainly concern us. The elastic bulk and shear moduli of the mixture are then calculated from its P- and S-wave transit times and density. The equations for these and subsequent calculations are given in the Appendix.

The moduli of the dry rock frame are calculated from Kuster and Toksöz' (1974) equations for evaluating the moduli of an elastic medium permeated with a dilute ($\phi \ll \alpha$) distribution of empty randomly oriented non-interacting ellipsoidal pores. We overcome the limitation on porosity by applying DEM theory (Xu and White 1995a), introducing the pores in steps, each step injecting a concentration small enough to satisfy the condition $\phi \ll \alpha$. The effective elastic moduli are updated using Kuster and Toksöz' (1974) equations and the updated moduli input to the next step, the process being repeated until the total porosity is reached.

In order to model transit times or velocities of low-frequency P- and S-waves, the moduli of the dry rock frame are input to the Gassmann (1951) model to simulate the effect of fluid relaxation. To model propagation at high frequencies, we dispense with Gassmann's (1951) theory and calculate the effective elastic moduli of the saturated rock by including the bulk modulus of the pore-fluid inclusions when applying the Kuster and Toksöz (1974) and DEM theories. This procedure assumes that fluid flow is the prime cause of velocity dispersion in rocks. It is based on the results of Mavko and Jizba (1991) and Mukerji and Mavko (1994) which show that Gassmann's (1951) equations are a low-frequency approximation whereas the theories of Hudson (1981) and Kuster and Toksöz (1974) which assume isolated pores are high-frequency approximations. In applying Kuster and Toksöz (1974) theory to derive the elastic moduli of dry rock frame, it does not matter whether the pores are connected or isolated because they are empty. In terms of the fluid-flow mechanisms, the subsequent application of Gassmann's (1951) theory makes this version of the model a low-frequency one, applicable to seismic modelling and possibly well-log analysis. In the high-frequency version of the model, there is no fluid flow between pores corresponding to only local stress relaxation inside each pore.

Our previous paper (Xu and White 1995a) demonstrated, using well logs and published laboratory measurements, how predictions from the clay–sand model explain much of the scatter commonly seen in porosity–velocity (P-wave) cross-plots from siliciclastic rocks. The model also simulates the two distinct porosity–velocity trends observed by Marion *et al.* (1992) for shaly sands and for sandy shales. Recently (Xu and White 1995b), we demonstrated that, whereas the low frequency was suitable for modelling logging data, the high-frequency model was more suitable for simulating laboratory measurements made at frequencies from hundreds of KHz to MHz. We use the appropriate version of the model in the comparisons of predictions and observations that follow.

We have also extended the model to simulate the anisotropic behaviour of shales

and sandy shales (Xu and White 1995c) by including an orientation distribution for pores associated with clays, similar to that proposed Hornby, Schwartz and Hudson (1994) for modelling pure shales. Details are left for a subsequent publication. Preliminary results show that the velocity behaviour of elastic waves travelling in directions perpendicular to the preferred orientation of the pores is close to that predicted by the isotropic model. The assumption of random orientation cannot be justified for clay-related pores and predictions from the isotropic model are intended for the vertical direction only.

The prediction of S-wave velocities in siliciclastic rocks is a natural extension of the model. Moreover prediction of S-wave velocity v_S requires the estimation of no parameters beyond those already employed in v_P prediction and achieves as good or better practical accuracy.

S-wave velocity and P-wave velocity, porosity and clay content

Results from laboratory measurements

Figure 2 shows measurements, made by Han *et al.* (1986) at 40 MPa confining pressure and 1 MPa pore pressure, that demonstrate how S-wave velocity decreases with porosity and clay content. There is indeed much laboratory evidence (e.g.

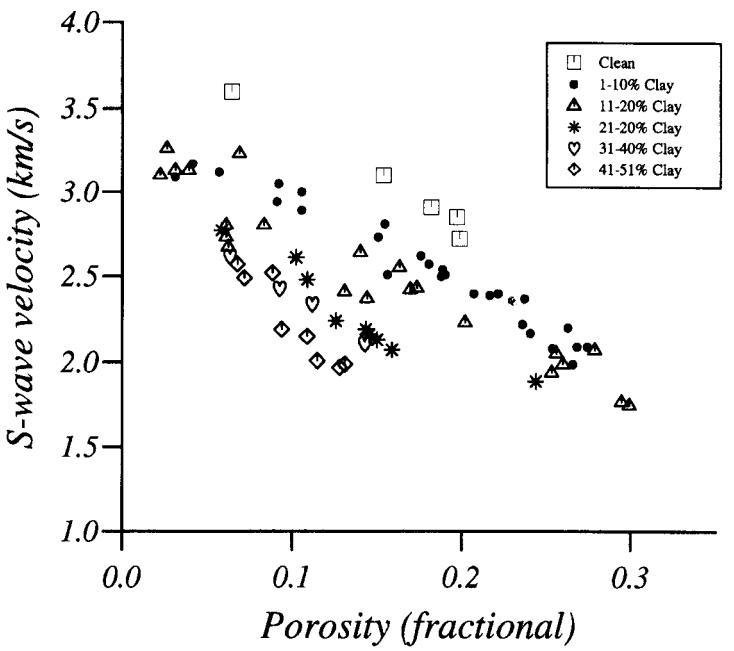

Figure 2. Illustration of the observed variation of S-wave velocity with porosity and clay content. Different symbols represent different volume fractions of clay content. Measurements are from Han *et al.* (1986).

Klimentos and McCann 1990; Klimentos 1991; Marion *et al.* 1992) to show that porosity and clay content affect elastic wave propagation significantly.

Figure 3 is a cross-plot of laboratory measurements of v_P and v_S made by Han *et al.* (1986) at 40 MPa confining pressure and Rafavich *et al.* (1984). It shows that the $v_P - v_S$ relationship for a given rock type is notably less scattered than that between v_S and porosity (Fig. 2). Figure 3 also illustrates the importance of lithology on the $v_P - v_S$ relationship. The clay–sand model can be adapted to predict this relationship for pure limestones (dashed line) and dolomite (dotted line) as well as sandstones (solid line) and these predictions are shown for reference. However we shall not consider limestones and dolomites. Our interest is clay–sand mixtures and especially the departure of the sandstone measurements from the clean sandstone line due to clay minerals in the rock samples.

As mentioned in the introduction, various linear relationships involving S-wave velocities or transit times have been put forward in the literature. There is evidence that non-linearity is a feature of unconsolidated rocks. Blangy and Nur (1992) restricted their linear relationship between shear modulus and porosity to consolidated rocks, with slope dependent on clay content. From laboratory measurements by Domenico (1976), Yin, Han and Nur (1988), Han *et al.* (1986)

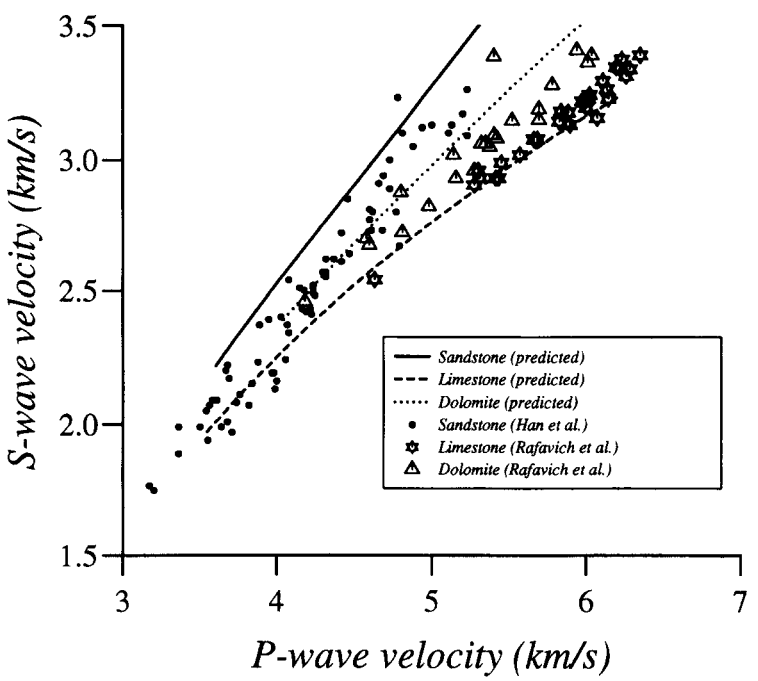

Figure 3. The $v_S - v_P$ relationship from the laboratory measurements (symbols) of Han *et al.* (1986) and Rafavich *et al.* (1984); the predicted relationships for pure lithologies are shown as lines.

and their own data, Blangy *et al.* (1993) found that the dry bulk modulus of a clean sandstone or shaly sandstone with less than 30% clay content could be approximated as a linear function of porosity with its slope changing with clay content, but the dry bulk modulus of a sandy shale (with clay content above 30%) or unconsolidated sands varied non-linearly with porosity.

These empirical equations cannot all be correct, except possibly under limited conditions. If v_S is a linear function of porosity, the relationship between S-wave transit time and porosity must be non-linear, and vice versa. It is of practical interest to establish where relationships are linear or approximately so. For practical purposes it is also important to understand the mutual relationships between those factors known to affect S-wave velocity, such as porosity, clay content, pressure, and temperature, and to isolate any dominant predictors of S-wave velocity in order to develop a more reliable empirical relationship.

Results from modelling

We use the clay–sand mixture model to study the relationships discussed above by calculating P- and S-wave velocities and transit times for a shaly sandstone as a function of porosity and clay content. The parameters used in these simulations are listed in Table 1. It should be noted that the P- and S-wave transit times for clay minerals are often not well established; the values used here are based on data published by Greenberg and Castagna (1992). The aspect ratios for sand- and clay-related pores are typical of the results in Xu and White (1995a).

Figure 4 shows the predicted S-wave velocity and transit time as a function of porosity and clay content (dotted lines) and the laboratory measurements (symbols), made by Han *et al.* (1986) at 40 MPa confining pressure and 1 MPa pore pressure. The results portray the relationship between S-wave velocity (or transit time) and porosity as generally non-linear, with the non-linearity increasing with clay content. Considering the range of porosity and scatter in the measurements in practice, it would be difficult to detect any non-linearity in either the $v_S-\phi$ or the $T^S-\phi$ relationship, except possibly for high clay contents. For a clean sandstone or sandstone with less than 10% clay content the $T^S-\phi$ relationship is virtually linear. This is consistent with the application of the time-average equation to clean or reservoir-quality sandstones. It is clear that the slope of any linear approximation depends on clay content.

Table 1. Transit times, density and aspect ratio for different rock types.

Lithology	T^P (μs/m)	T^S (μs/m)	Density (kg/m^3)	Aspect ratio
Sandstone	171	256	2650	0.12
Shale	230	394	2600	0.03
Brine	617		1050	

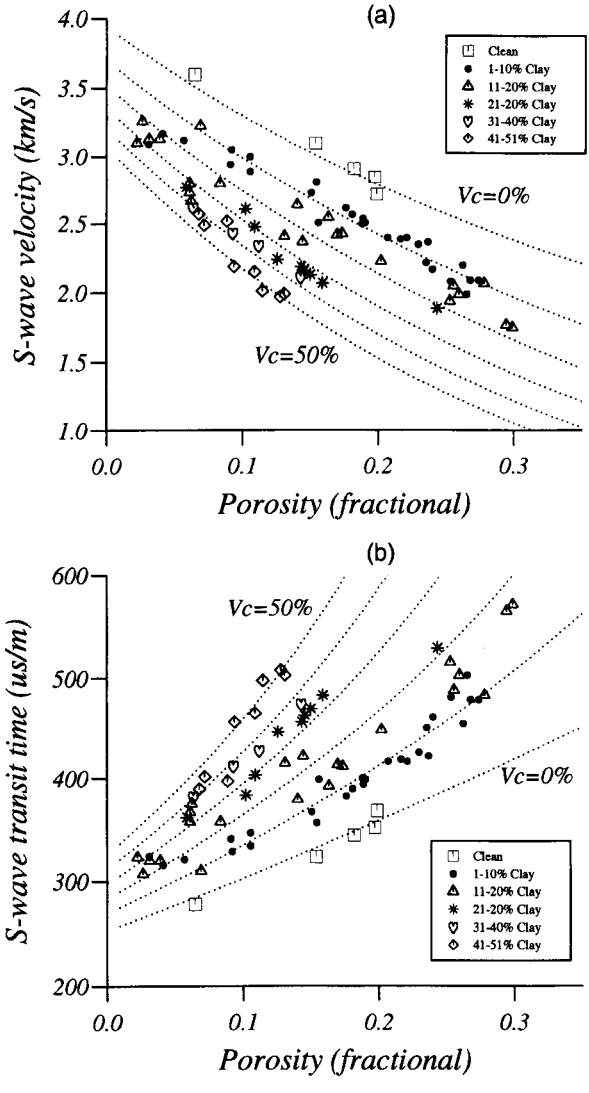

Figure 4. (a) S-wave velocity and (b) S-wave transit time as a function of porosity and clay content, calculated using the clay–sand mixture model (dotted lines). The various symbols represent the measurements of Han *et al.* (1986) at 40 MPa confining pressure for various volume fractions of clay content. Model parameters are listed in Table 1.

These results suggest that linearity may be a reasonable approximation when the clay content is less than, say, 30% but that it is not applicable when both porosity and clay content are significantly high. Of course the model must accord with observations for these conclusions to be valid but comparison of the measurements and the predictions shows that the model is simulating laboratory observations rather

well. As further evidence we show in Fig. 5 the $v_P - v_S$ relationship predicted from the model. The dotted lines correspond to curves calculated for values of the normalized shale volume (as a fraction of the total volume of the grain matrix) ranging from 0 (clean sands) to 1.0 (pure shale) in steps of 0.2. The laboratory measurements of Han *et al.* (1986) at confining pressure of 40 MPa are plotted on the diagram for comparison. The clay content in these sandstone samples varied from 0% to 51%. The solid line is the well-known mudrock line for siliciclastic rocks of Castagna *et al.* (1985).

These simulations indicate that for brine-saturated siliciclastic rocks, S-wave velocity can be expressed as a linear function of P-wave velocity. The slope and intercept are related and depend on clay content. In a more general context, we expect the slope and intercept to depend on pore geometry. Figure 5 accords with the suggestion of Greenberg and Castagna (1992) that the relationship between S- and P-wave velocities is more robust and less sensitive to clay content than that between S-wave velocity and porosity (see also Figs 2 and 3). Evidently P- and S-wave velocities are both affected by porosity and clay content as well as lithology.

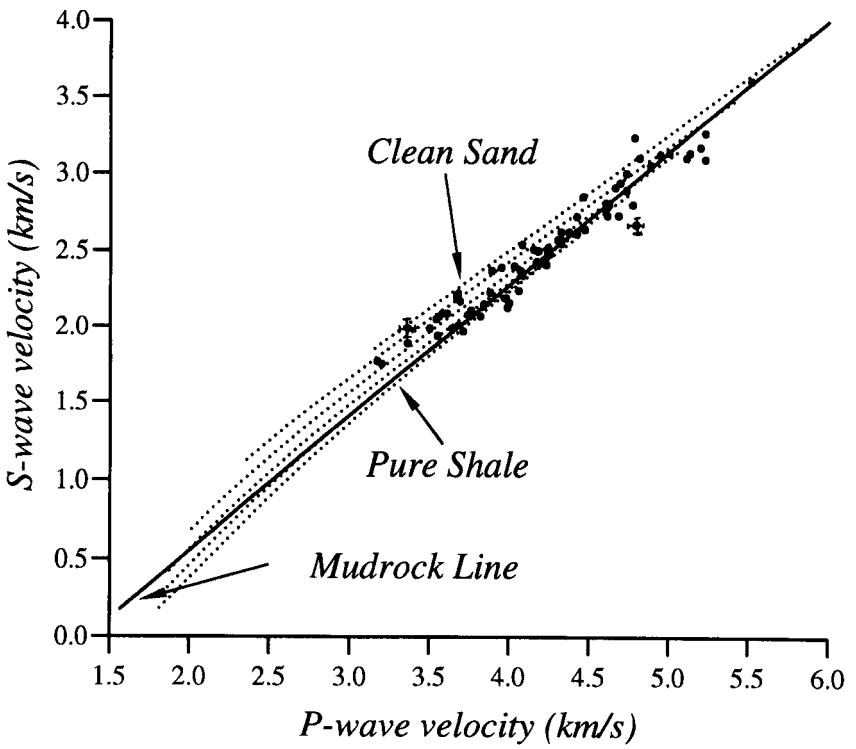

Figure 5. The relationship between P-wave and S-wave velocities predicted as a function of clay content (dotted lines: clay content varying from clean sand to 'pure' shale downwards) and comparison with laboratory measurements at 40 MPa confining pressures (solid circles) from Han *et al.* (1986). The solid line is Castagna's (1985) mudrock line.

Figure 6 compares the dry shear modulus predicted from the model and the laboratory measurements presented by Blangy *et al.* (1993). Again the prediction shows a general non-linear relationship between the dry shear modulus and porosity, with the non-linearity increasing with clay content. The results also show that the first few percent of clay content have a stronger effect on the elastic properties of clay–sand mixtures. This agrees with the conclusion drawn by Blangy *et al.* (1993).

Two other factors that affect P- and S-wave velocities are cementation and consolidation. Although these factors are not readily quantified, a model based on aspect ratios offers some qualitative explanation of their effect. Where cementation fills small gaps, it tends to increase aspect ratio, thereby making linear relationships more likely. On the other hand the elastic behaviour of unconsolidated rocks, which contain a large number of unclosed small gaps between grain boundaries, is likely to be dominated by small aspect ratios, leading to a non-linear porosity–velocity relationship. These small gaps, being the weakest 'springs', tend to close first under compaction. The presence of these compliant pores makes unconsolidated sands behave like shales. This helps to explain why Blangy *et al.* (1993) classified shales and unconsolidated sands into the same group.

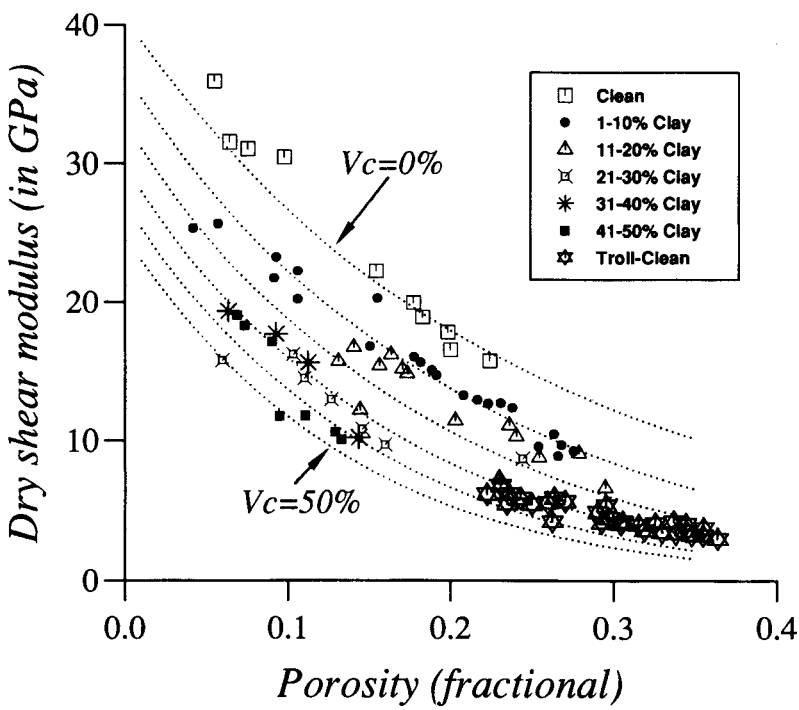

Figure 6. Comparison of the measured dry shear modulus (symbols) and that predicted from the clay–sand mixture model (solid lines). The measurements were redrafted from Blangy *et al.* (1993). Parameters used in the simulation are listed in Table 1.

Shear-wave velocity prediction

Procedure

The model can predict S-wave velocity using measurements of

1. grain matrix parameters (lithology), porosity and clay content (Fig. 4),
2. lithology, P-wave velocity and clay content (Fig. 5), or
3. lithology, P-wave velocity and porosity (Xu and White 1995b).

If all the measurements are error free, it does not matter which scheme is used. In practice schemes 2 or 3 should be used because

(a) there is a very good correlation between v_P and v_S: both are similarly affected by porosity, clay content and lithology; and

(b) the sonic log is usually more reliable than estimates of porosity and shale volume for which errors, besides those involved in the measurements, may be introduced due to the use of imperfect models and imperfect parameters.

Xu and White (1995b) illustrate how comparison of the S-wave logs predicted from schemes 2 and 3 helps check the consistency of the model and identify unreliable portions of log. Here we confine ourselves to the use of scheme 2.

Figure 5 provides the basis for scheme 2. It shows that S-wave velocity can be predicted from P-wave velocity and clay content. This does not mean that S-wave velocity is independent of porosity. Rather the P-wave velocity contains all the information about porosity needed to predict S-wave velocity.

Figure 5 also shows to what degree our model can improve the v_S prediction over Castagna's (1985) mudrock line. For P-wave velocities, say higher than 4.5 km/s, the maximum correction is less than 8% and there is little advantage over Castagna's (1985) mudrock line unless the errors in P-wave velocity are some fraction of this (the fraction depends on the accuracy of the clay content). On the other hand, for low P-wave velocities (high porosities), the improvement may be significant, depending on the variations in clay content.

Comparison with laboratory measurements

We use the laboratory measurements made by Han *et al.* (1986) at 5 MPa confining pressure and 1 MPa pore pressure to study the validity of the model. Figure 7 shows cross-plots of the measured and predicted S-wave velocities using (a) porosity and clay content and (b) P-wave velocity and clay content. The smaller scatter in Fig. 7b confirms the robust relationship between P- and S-wave velocities stated above and indicates the degree of improvement obtained from the model. Parameters used in the S-wave prediction are listed in Table 1 except that the best-fit aspect ratios were 0.08 for sand-related pores and 0.02 for clay-related pores. These lower values can be attributed to the reduced effective pressure which allows pores with low aspect ratios,

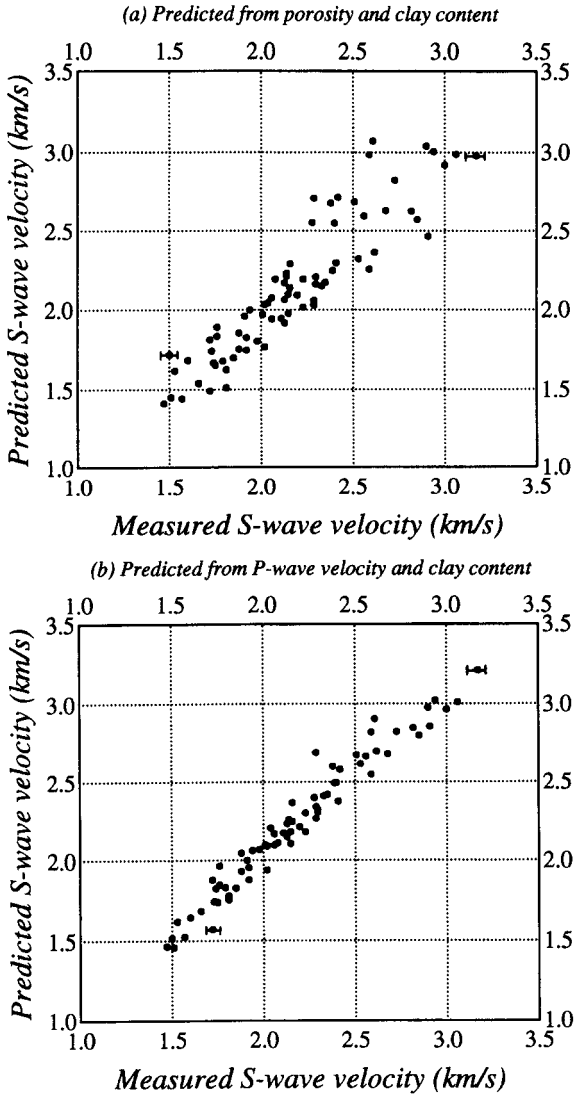

Figure 7. Cross-plot of measured S-wave velocities against predictions from (a) porosity and clay content and (b) P-wave velocity and clay content. The measurements were made from 75 samples at 5 MPa confining pressure by Han *et al.* (1986).

or cracks, to remain open, thereby reducing the mean aspect ratios for sand- and clay-related pores. The best-fit aspect ratios for modelling the measurements at 40 MPa confining pressure (Han *et al.* 1986) were the same as those tabulated in Table 1. The results at 5 MPa are more scattered than those at 40 MPa, presumably because of microcracks, and make a sterner test of the model.

Comparison with log data

We also applied the model to P- and S-wave logs from two wells provided by BP. Before giving results, we discuss how to determine the required parameters from well-log analysts and how they affect velocity predictions.

Guidelines for parameter determination

Published data (e.g. Serra 1984, p. 225) show very little variation in densities, P- and S-wave transit times for brine and for lithologies without porosity such as tight sandstone, limestone and dolomite. Although factors such as cementation, temperature, pressure, etc., may affect these parameters, the effects are relatively small in comparison with other factors described below. (It is possible to classify cement as a lithology, but we do not do it because it is hard to identify cement type and cement volume from a normal log analysis). The parameters for sand grains and brine are therefore based on published tables. Values for oil and gas can also be found from tables but must be corrected for temperature and pressure.

The parameters for the clay particles must be checked for consistency with the logs. First of all there are few published values for the P- and S-wave velocities and densities of different clay minerals. Secondly, in practical formation evaluation, log analysts normally evaluate shale volume instead of clay content and there are a number of problems in determining shale volume.

1. It is often uncertain what types of clay minerals the shale contains.
2. Shale consists of silts as well as clay minerals and the volume of the silts can, on occasion, be more than 50% of the total volume.
3. Shale, however pure it is, contains a certain amount of bound water and/or hydration water.
4. A 'pure' shale defined by gamma-ray or other logs may be overpressured or poorly compacted; it is likely to contain some residual porosity.
5. Changes in hole size can alter the response of the gamma-ray tool, making it difficult to ensure consistent estimation of shale volume over different log intervals.
6. Different relationships have been proposed for converting gamma-ray readings into shale volume; we generally use the non-linear relationship of Rider (1991, p. 66) for pre-Tertiary consolidated rocks.

Given these uncertainties, which are by no means atypical of log analysis in shaly intervals, estimation of shale parameters has to rely on careful assessment of the logs and is better illustrated by example than by proposing an artificial 'cut-and-dried' procedure. These uncertainties are compounded by the strong coupling between the parameters adopted for the shale and the clay-related aspect ratio, although the coupling does not greatly hamper v_S prediction in practice.

In many wells parameters for a 'pure' shale can be found on the gamma-ray log from a deep well-compacted shale. This was so in case study 1 below, which illustrates how the shale parameters can be estimated. The parameters from a 'pure'

shale zone defined from the gamma-ray log at depths around 2895 m in Well A of this case study are listed in Table 2. The table also lists the density and P-wave transit time of a well-compacted shale in well 44/29-1A in the southern North Sea (Xu and White 1995a). These values are close to those given by Greenberg and Castagna (1992) for illite and a corresponding value for the S-wave transit time was assigned to this shale on the basis of this similarity. Although they may change from area to area or even from well to well, such tabulated shale parameters are a useful guide for deciding whether a selected 'pure' shale zone contains significant residual porosity. The relatively high P-wave transit time and low density at Well A suggest that a certain amount of residual porosity is present. The values are consistent with the assumption that the residual porosity for this shale zone is about 11% and the P-wave transit time and density for the corresponding 'pure' shale without residual porosity are 230 μs/m and 2600 kg/m^3. By correcting the gamma-ray and neutron logs for this 11% porosity, corrected log values for the shale without residual porosity can be obtained (see Table 2). In summary the shale parameters were estimated by trial-and-error calculations using comparable tabulated and field parameters.

There are two options for choosing shale parameters for velocity prediction in this example: (1) using original log values and (2) using corrected log values. The former are compromised by any residual porosity and the latter by uncertainties in the correction. As the presence of porosity makes the shale appear more compliant than its clay minerals really are, the model requires a larger (less compliant) aspect ratio than one with the correct shale parameters. Nevertheless use of the original log values gave a slightly better fit in case study 1.

Porosity is evaluated by a standard method using the Well Data System log analysis package. A reliable estimate of porosity is important to the method and as many logs as are available are used. A density log is essential and a neutron porosity log over at least some interval; deep resistivity logs, which are generally run, can also provide estimates of porosity where brine properties are known. The best check is comparison of the porosity log with core measurements. Given a reliable porosity log, it is possible to compute a pseudoshale-volume log from the P-wave transit times (Xu and White 1995b) and this can be helpful in identifying problems in the shale-volume estimates.

Table 2. Log values of a 'pure' shale before and after correction for effective porosity.

Log type	(Unit)	Log values (before correction)	Log values (after correction)
GR	(API)	98	108
RHOB	(kg/m^3)	2450	2600
NPHI		0.45	0.40
DT (P-wave)	(μs/m)	341	230
DT (S-wave)	(μs/m)	689	394

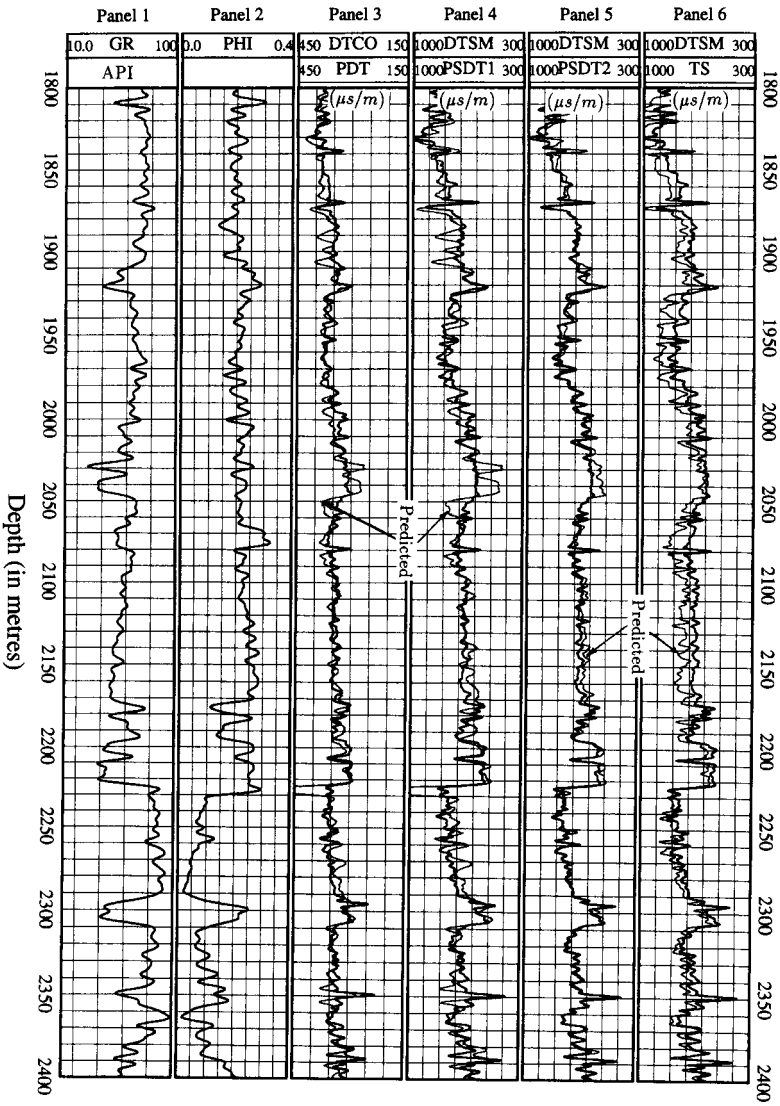

Figure 8. Comparison of the measured P- and S-wave transit times and those predicted from the clay–sand mixture model and Castagna's (1985) mudrock line. Shale parameters come from log values read from the selected shale zone without porosity correction (see Table 2). Aspect ratios for sand- and clay-related pores are 0.12 and 0.05 respectively. Other parameters are the same as those listed in Table 1. GR: gamma-ray; PHI: porosity; DTCO: measured P-wave sonic log; PDT: predicted P-wave log; DTSM: measured S-wave sonic log (dipole); PSDT1; S log predicted from porosity and shale volume; PSDT2: S log predicted from P-wave log (DTCO) and shale volume; TS: S log predicted from the mudrock line.

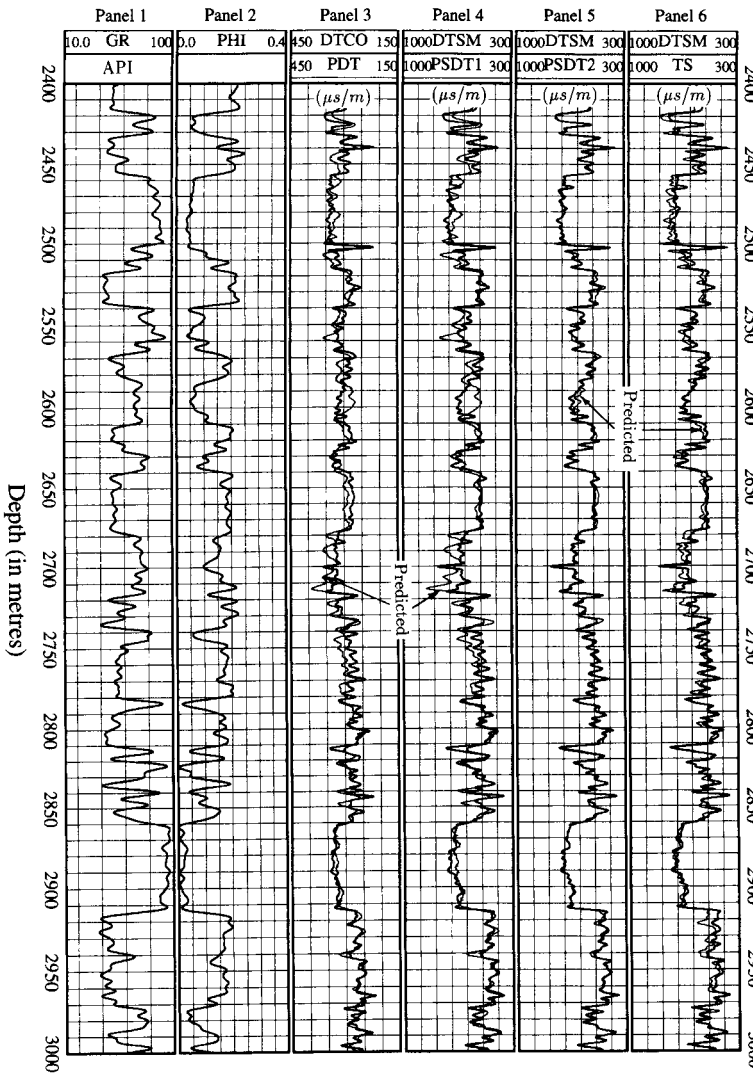

Figure 8. Continued.

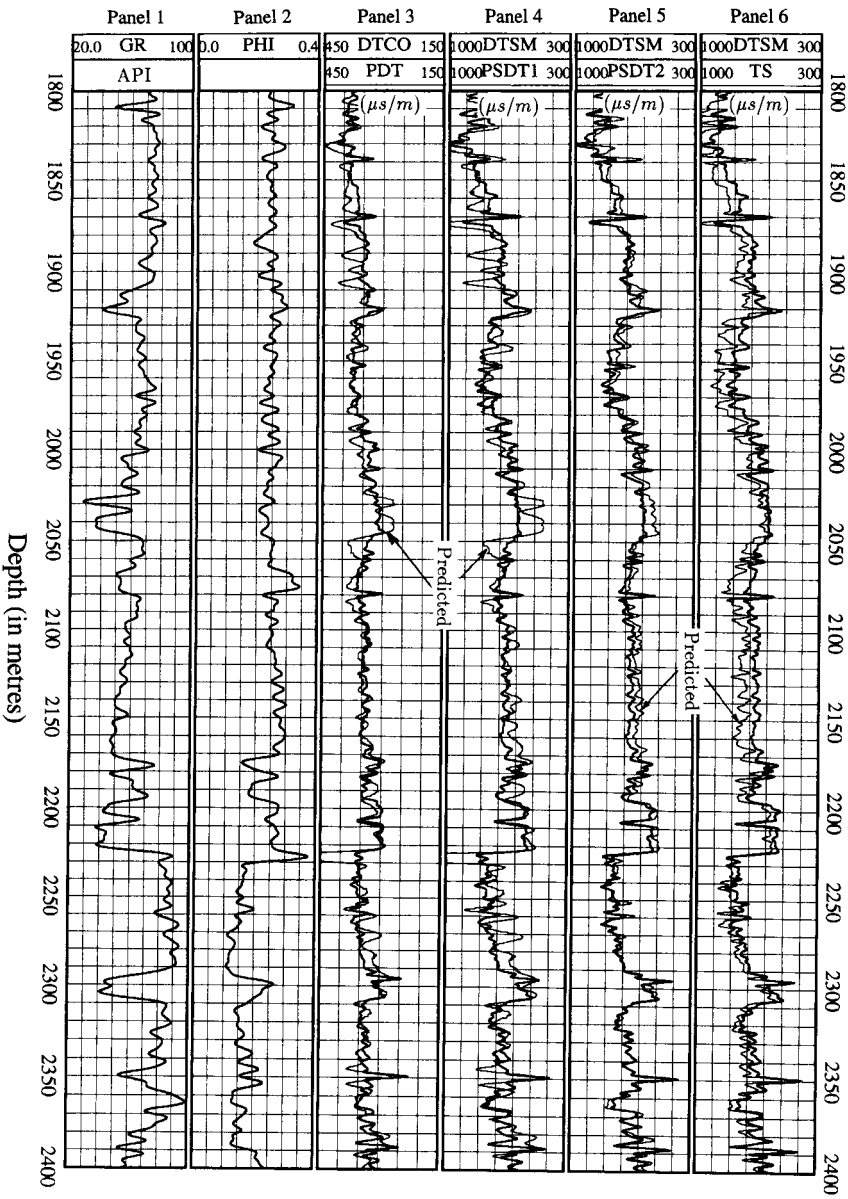

Figure 9. Comparison of the measured P- and S-wave transit times and those predicted from the clay–sand mixture model and Castagna's (1985) mudrock line. Shale parameters come from log values corrected for the residual porosity contained in the selected shale zone (see Table 2). Aspect ratios for sand- and clay-related pores are 0.12 and 0.03, respectively. Other parameters are the same as those listed in Table 1. Notations are the same as those for Fig. 8.

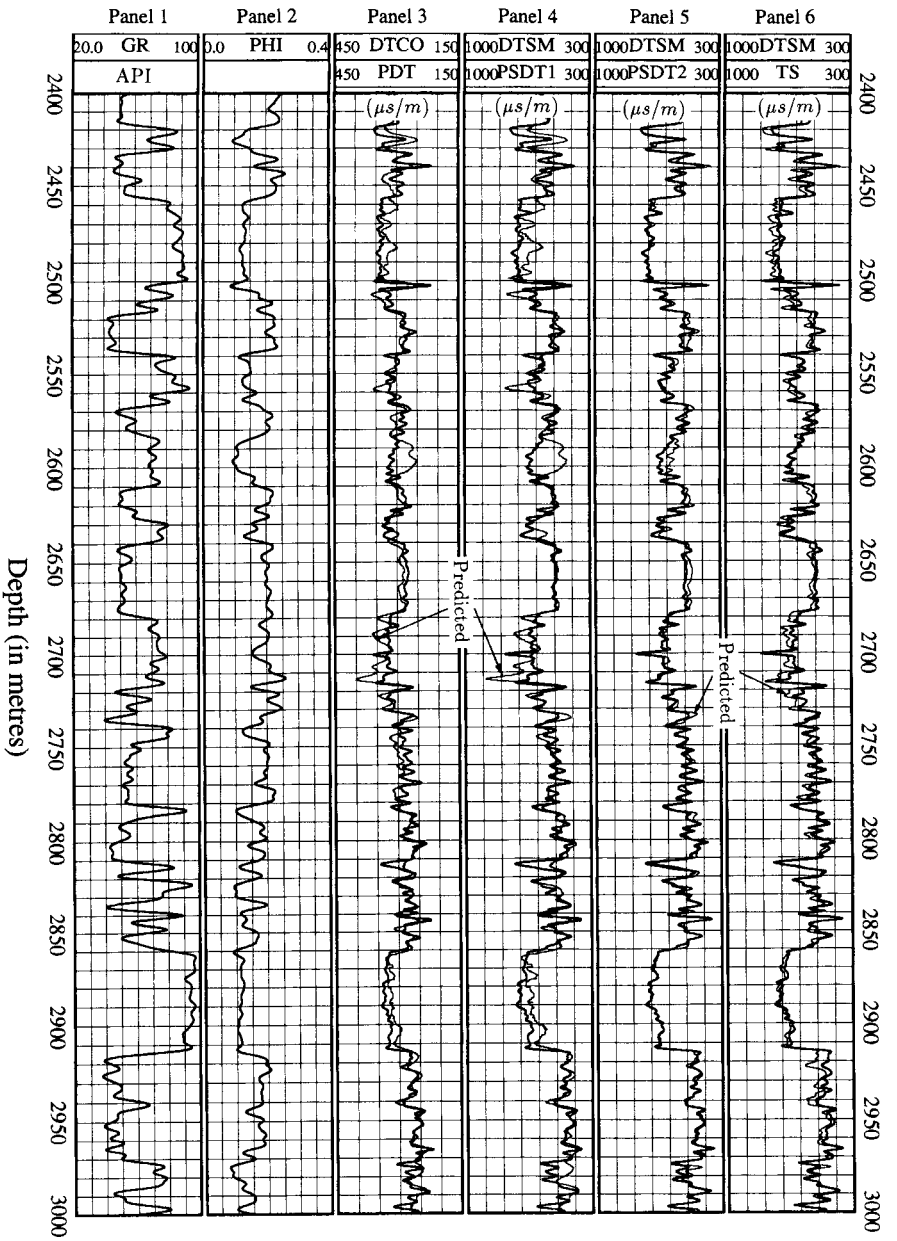

Figure 9. Continued.

Once the porosity has been evaluated and the shale parameters chosen, the estimation of aspect ratios is relatively straightforward since it simply relies on making a best fit. With just two parameters to be estimated, the procedure could be readily automated. However we prefer a visual approach that can take account of specific problems in the logs and concentrate on sandy intervals when tuning α_S guided by the normalized mean-square error (NMSE, Xu and White 1995a) between the observed and predicted logs. Trials to date have consistently yielded aspect ratios close to 0.10 for the sand component and around 0.02–0.05 for the clay component. We noted above that the best-fit aspect ratio for clay-related pores depends on how the 'pure' shale zone was selected.

Although it would be helpful to have independent estimates of the effective aspect ratios of sand-related and clay-related pores, there is no ready way of obtaining them. The aspect ratios employed by the model characterize the elastic behaviour of the two solid components and their differing response to porosity. In effect the model uses a bimodal distribution of pores, with concentrations determined by the normalized sand volume and clay content. Whatever its defects in the abstract, the model has been tried in blind tests and succeeded just as well in predicting v_S in these as in the two case studies reported below. Given a sufficient base of well data, it may be possible to relate aspect ratios to other parameters such as effective pressure.

Case 1: Well A

Figure 8 shows a comparison of the measured P- and S-wave sonic logs at this well with the model predictions using 'pure' shale parameters directly read from logs at the selected shale zone. Figure 9 shows the comparison with predictions using corrected shale parameters. The same parameters for sand grains and pore fluid (Table 1) are applied in both cases. The gamma-ray log is presented in Panel 1 and the porosity log estimated from the density log is shown in Panel 2. Panel 3 compares the measured P-wave transit times (DTCO) and those predicted from our model (PDT). Panels 4 to 6 show the comparisons between the measured S-wave transit times and those predicted from porosity and shale volume (PSDT1 in Panel 4), from P-wave transit time (DTCO) and shale volume (PSDT2 in Panel 5) and from Castagna's (1985) mudrock line (TS in Panel 6).

The two figures illustrate some important points.

1. Prediction of S-wave velocity from P-wave velocity and shale volume is more reliable than prediction from porosity and shale volume. The reasons for this were explained in the previous section.

2. Castagna's (1985) mudrock line works well for shaly formations with less than 20% porosity but underestimates transit times when the porosity exceeds 20% (NMSE = 0.117). This accords with the results shown in Fig. 5.

3. The aspect ratio for sand-related pores is stable at 0.12 but the aspect ratio for clay-related pores depends also on how one defines a 'pure' shale line. When 'pure' shale values are read directly from the selected shale zone, the best-fit aspect ratio for

clay-related pores appears to be 0.05; after correcting the 'pure' shale log values for porosity, the best-fit aspect ratio is about 0.03.

4. The predictions from uncorrected shale values (NMSE = 0.050) are somewhat better than those from corrected shale values (NMSE = 0.059). But, despite the coupling between the shale parameters and the clay-related aspect ratio, both provide acceptable predictions.

Case 2: Well B

No gamma-ray log was provided for Well B. Instead there is a shale volume curve which suggests an almost 'pure' shale zone over the depth interval of 3880 to 3900 m. 'Pure' shale lines for NPHI (neutron), RHOB (density), DT (P-wave transit time) and DTSB (S-wave transit time) can be obtained from the corresponding logs over the same depth interval. Table 3 tabulates the parameters used for velocity prediction. On the basis of the previous case study, uncorrected shale readings were used in the velocity prediction and the S-wave log was predicted from DT and VSH. Both P-wave transit time and density read from the selected 'pure' shale zone suggest that some residual porosity remains, which would again lead to overestimation of the aspect ratio for clay-related pores.

The predicted S-wave transit times fit the observations extremely well (Fig. 10, NMSE = 0.04). A sensitivity study of parameters shows that changes of 10% in aspect ratios affect the predicted P-wave transit times by about 4% but the predicted S-wave transit times by only 1%. This does not mean that S-wave transit time is insensitive to pore geometry but that, when predicting v_S from v_P, the effect of geometry is contained in the P-wave transit time.

Effect of water saturation on v_P/v_S ratios

Wood's (1941) suspension model can be used to estimate the effective bulk modulus of the pore-fluid mixture (Domenico 1976; Greenberg and Castagna 1992) in partially saturated rocks:

$$\frac{1}{K_f} = \frac{1 - S_w - S_o}{K_a} + \frac{S_w}{K_w} + \frac{S_o}{K_o} \tag{1}$$

Table 3. Parameters used for predicting P- and S-wave transit times at Well B.

Lithology	T^P (μs/m)	T^S (μs/m)	Density (kg/m^3)	Aspect ratio
Sandstone	171	256	2650	0.12
Shale	341	584	2450	0.04
Brine	617		1050	

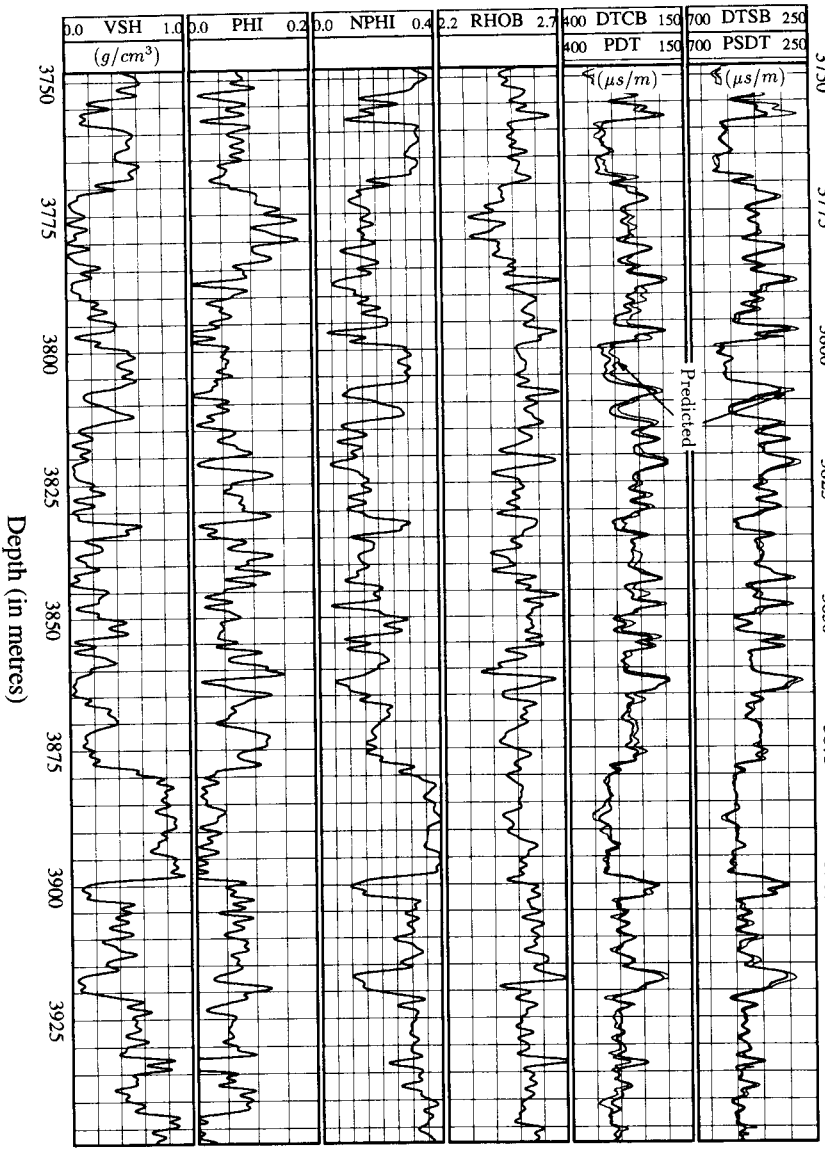

Figure 10. Comparison of the measured P- and S-wave transit times and those predicted from the clay–sand mixture model at Well B. Parameters used in the prediction are listed in Table 3. VSH: shale volume; PHI: porosity; NPHI: neutron porosity; RHOB: bulk density; DTCB: measured P-wave sonic log; PDT: predicted P-wave log; DTSB: measured S-wave log (dipole); PSDT: S-wave log predicted using DT and VSH.

and

$$\rho_f = (1 - S_w - S_o)\rho_a + S_w\rho_w + S_o\rho_o, \tag{2}$$

where K_a, K_w and K_o are the bulk moduli of the gas, water (or brine) and oil, and ρ_a, ρ_w and ρ_o are the corresponding densities. S_w and S_o denote the saturation of water and that of oil.

Domenico (1976) and Gist (1994) maintain that both Gassmann's (1951) theory and the effective fluid compressibility calculated by volume-weighted average of the gas and brine compressibilities can apply only to low-frequency seismic velocity measurements. Domenico (1976) stated that although brine saturation is macroscopically distributed, the gas and brine are not in the same proportion in each pore space since the amount of gas or brine in each pore depends on pore size and the wettability of the material. At high frequencies the stress field passes through rock samples saturated with gas and brine so quickly that there is no time for a proportion of gas and brine to interact with each other. The study of the saturation dependence of high-frequency velocity measurements needs detailed information about pore-size distribution, wettability of the matrix, which is obviously beyond the scope of our model. Here we simply show how clay content (compliant pores) can magnify the effect of water saturation on low-frequency velocities. Seismic exploration and sonic logging are considered to be low-frequency experiments because their wavelengths are so much larger than pore sizes.

Two simple examples show the effect of water saturation on P- and S-wave velocities. Calculations were carried out assuming that the rock under study was (a) a clean sandstone and (b) a shaly sandstone with 30% clay content. In both cases the rock is further assumed to be saturated with brine and gas and to have 22% porosity. Table 4 lists the other parameters in these calculations. Figure 11 shows the results. The slow decrease in P- and S-wave velocities with increasing water saturation is mainly due to the increase in density. However, after S_w reaches a certain value (about 99%), the P-wave velocity increases sharply. At laboratory frequencies, the increase in P-wave velocity normally starts at about 80% water saturation (Domenico 1976; Knight and Nolen-Hoeksema 1990) but it has been confirmed by laboratory measurements at seismic frequencies (Murphy 1984).

A very important conclusion from comparison of parts (a) and (b) of Fig. 11 is that clay content increases the size of the jump in P-wave velocity near 99% water saturation. The stiff pores of clean sandstone inhibit compressions and rarefactions

Table 4. Parameters used to calculate the effect of saturation on P- and S-wave velocities.

Lithology	T^P (μs/m)	T^S (μs/m)	Density (kg/m^3)	Aspect ratio
Sandstone	171	256	2650	0.12
Shale	230	394	2600	0.02
Brine	617		1050	
Gas	3025		1.29	

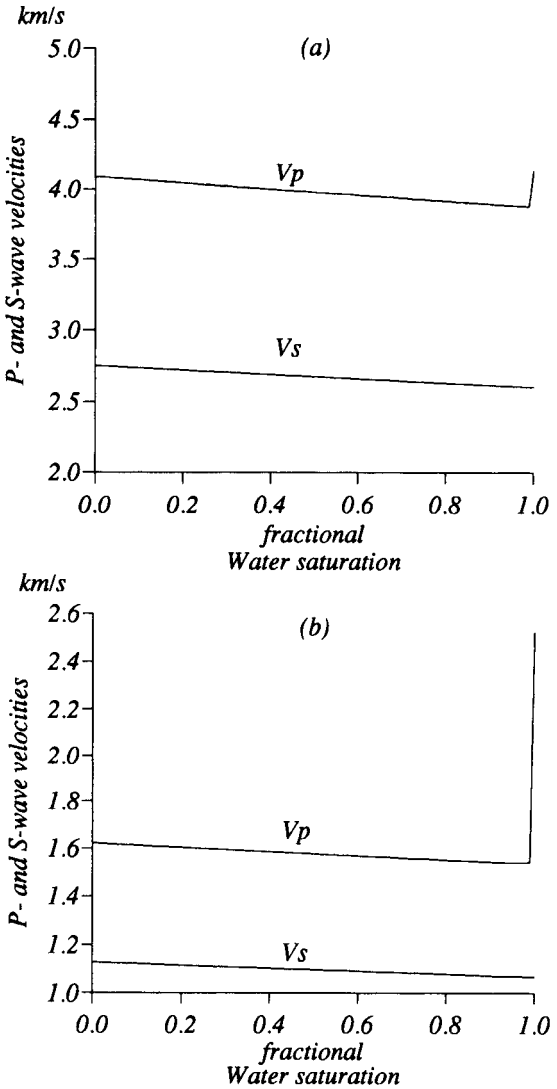

Figure 11. Illustration of the effect of water saturation on P- and S-wave velocities. The other fluid is assumed to be gas and the rock is assumed to be (a) clean sandstone and (b) a shaly sandstone with 30% clay content. In both cases the porosity is assumed to be 22%. Parameters are listed in Table 4.

of the pore fluid whereas the compliant pores in a shaly sandstone allow the wavefield to 'see' the compressibility of the pore fluid. Thus gas is more likely to be detected from logging and seismic data in unconsolidated or shaly formations than in clean and consolidated formations.

We have not found experimental data to confirm or deny the effect of clay content

predicted by the simulations in Fig. 11. However a similar effect is seen in the interaction between water saturation and the application of pressure to rocks containing microcracks. Figure 12 (after Winkler and Nur 1982) shows the P- and S-wave velocities in dry (D), partially (roughly 90%) saturated (PS) and fully saturated (FS) Massillon sandstone and, in effect, displays as a function of effective pressure, three P- and S-wave velocities corresponding to S_w values of 0%, an intermediate value and 100% in Fig. 11. The difference in P-wave velocities in the dry and fully saturated states decreases with effective stress, suggesting a loss of compliant pores from the closing of microcracks, which respond in a similar way to pores with very small aspect ratios. Figure 12 implies that at 300 bars the sandstone contains only pores with fairly large aspect ratios.

Discussion

The clay–sand mixture model simulates both P- and S-wave velocities over the full range of siliciclastic rocks from clean sandstones to pure shales, whether consolidated or moderately unconsolidated. In comparison with the simplest alternative, the time-average model (which is restricted in application to clean consolidated sandstones), it requires just two extra parameters: the effective aspect ratios for sand-related and clay-related pores. The mixture model employs fewer data-dependent parameters

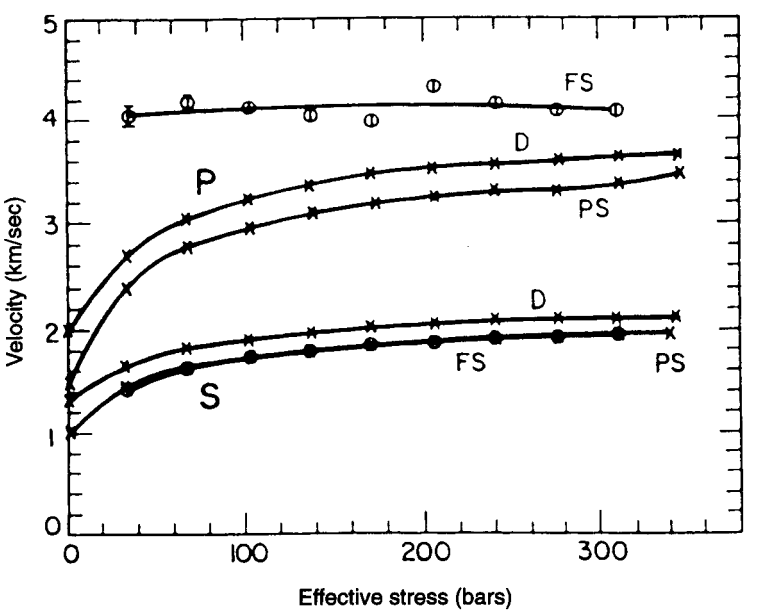

Figure 12. Illustration of the effect of water saturation and effective stress on wave velocities in Massillon sandstone, after Winkler and Nur (1982); notation: D–dry, PS–partially saturated (90%), FS–fully saturated.

than linear regressions which require at least four parameters to predict both P- and S-wave velocities (six if the constants, which should equal the grain-matrix velocities, are included). Moreover the range of validity of regressions is more limited and their predictions are generally less accurate than those of the clay–sand model. The model thus provides the capability of accurate prediction in a very efficient manner with no artificial breaks between, say, shaly sands and sandy shales. It requires only two fitted parameters (three if the residual porosity of 'pure' shale is included) to predict both P- and S-wave velocities.

Unlike empirical models and, say, the successful semi-empirical model of Greenberg and Castagna (1992), the clay–sand model avoids the need for large amounts of data to establish the empirical relationship between S- and P-wave velocities for fully saturated rock. This makes the clay–sand model less dependent on the availability of a large data base and the appropriateness of that data base to specific case studies.

In addition to its efficient predictive capabilities and its adaptability to the problem in hand, the clay–sand model has other applications besides S-wave velocity prediction. It is well suited to undertaking fluid substitution studies. Xu and White (1995b) describe how the use of two schemes for S-wave prediction provides a means of checking the consistency of its results and this can be of use in quality control of the logs employed in the prediction and show how laboratory measurements are simulated better by the high-frequency version of the model.

The main problem in application of the model comes from establishing suitable grain-matrix parameters for a 'pure' shale. This is as much a problem of interpretation of shaly intervals from log data as it is a problem of the model. At the conceptual level there are fundamental questions, such as the problem of independent validation of the estimated aspect ratios and the validity of partitioning the porosity into sand-related and clay-related components, which could generate extended discussion. In practice the aspect ratios are the right order of magnitude and the partition of the compliance into two components does provide accurate prediction in a very effective way.

Conclusions

1. According to the clay–sand mixture model, neither S-wave velocity nor S-wave transit time is strictly a linear function of porosity and clay content. If the model is accurate, empirical linear equations can predict S-wave velocity only over limited ranges of porosity and clay content. For a clean sandstone or sandstone with less than 10% clay content, the $T^S-\phi$ relationship is virtually linear. This is consistent with the application of the time-average equation to clean or reservoir-quality sandstones. The model predicts that clays are the main cause of non-linearity in relationships between dry moduli and porosity.

2. The model has been used to predict S-wave velocity. Comparisons of laboratory and logging measurements with predictions show that the relationship between

S- and P-wave velocities is more robust than that between S-wave velocity and porosity. Thus prediction from P-wave velocity and clay content is more reliable than that from porosity and clay content, although the same theory is used in both cases.

3. The model has the ability to show the effect of water saturation (S_w) on P- and S-wave velocities, and hence on v_P/v_S. Numerical results indicate that at low frequencies P- and S-wave velocities decrease slowly with increasing water saturation (increasing density) until S_w reaches a value near 99%, when the P-wave velocity increases sharply. The magnitude of the sharp increase depends significantly on clay content. Because we simulate the effect of clay content using compliant pores (pores with small aspect ratios), it can be concluded that it is compliant pores that predominantly control the saturation behaviour. There is some laboratory evidence that supports this prediction but, in view of its importance as a direct hydrocarbon indicator, further experimental investigation would seem well worthwhile.

Acknowledgements

The authors are indebted to the sponsors of the Birkbeck College Research Programme in Exploration Seismology, namely Amoco (UK) Exploration Company, BP Exploration Operating Company Ltd., Enterprise Oil plc, Fina Exploration Ltd., GECO Geophysical Company Ltd., Mobil North Sea Ltd., Sun Oil Britain Ltd. and Texaco Britain Ltd. for their support of this research, and to geophysicists and petrophysicists from these companies for helpful discussions and encouragement.

Appendix

Evaluation of sand-related and clay-related pore volumes

The sum of the pore volume related to sand grains, ϕ_s, and that related to clays, ϕ_c, is equal to the total pore space, i.e.

$$\phi = \phi_s + \phi_c. \tag{A1}$$

It is assumed that, to a first order approximation, ϕ_s and ϕ_c are proportional to sand-grain volume and clay content, i.e.

$$\phi_s = V_s \frac{\phi}{1-\phi} \tag{A2}$$

and

$$\phi_c = V_c \frac{\phi}{1-\phi}, \tag{A3}$$

where ϕ is the total porosity. V_c denotes the fractional clay volume, and V_s the fractional sand volume, as estimated from $V_s = 1 - \phi - V_c$.

Time-average and density equations

$$T_m^P = (1 - V_c')T_g^P + V_g' T_c^P \tag{A4}$$

and

$$T_m^S = (1 - V_c')T_g^S + V_c' T_c^S. \tag{A5}$$

The density is found from

$$\rho_m = (1 - V_c')\rho_g + V_c' \rho_c. \tag{A6}$$

In these equations T_g^P, T_c^P and T_m^P are the P-wave transit times of the sand grains, clay minerals and the mixture, T_g^S, T_c^S and T_m^S are the corresponding S-wave transit times and ρ_g, ρ_c and ρ_m the corresponding densities. V_c' is the clay volume normalized by the volume of solid matrix:

$$V_c' = \frac{V_c}{1 - \phi}. \tag{A7}$$

Calculation of elastic moduli

The elastic bulk and shear moduli of the grain mixture are calculated from its transit times using

$$K_m = \rho_m \left(\frac{1}{(T_m^P)^2} + \frac{4}{3(T_m^S)^2} \right) \tag{A8}$$

and

$$\mu_m = \rho_m \left(\frac{1}{(T_m^S)^2} \right). \tag{A9}$$

Kuster and Toksöz (1974) give equations for evaluating the moduli of an elastic medium permeated with a dilute ($\phi \ll \alpha$) distribution of (non-interacting) ellipsoidal pores:

$$K_d = \frac{K_m + 4A\mu_m}{1 - 3A} \tag{A10}$$

and

$$\mu_d = \mu_m \frac{1 + B(9K_m + 8\mu_m)}{1 - 6B(K_m + 2\mu_m)}, \tag{A11}$$

where

$$A = \frac{1}{3} \frac{K' - K_m}{3K_m + 4\mu_m} \sum_{l=s,c} \phi_l T_{iijj}(\alpha_l), \tag{A12}$$

$$B = \frac{1}{25} \frac{(\mu' - \mu_m)}{\mu_m(3K_m + 4\mu_m)} \sum_{l=s,c} \phi_l \left(T_{ijij}(\alpha_l) - \frac{T_{iijj}(\alpha_l)}{3} \right), \tag{A13}$$

K_d, K_m and K' are the bulk moduli of the dry frame, the mixture and the fluid and μ_d, μ_m and μ' are the corresponding shear moduli. K' and μ' are zero when computing the moduli of the dry frame (with empty pores). The scalars T_{iijj} and T_{ijij} are functions of the aspect ratio of the inclusions and the moduli and densities of the matrix and the fluid enclosed. The explicit expressions, given in Appendix B of Xu and White (1995a), correct a misprint in the equation for T_{iijj} in the original Kuster and Toksöz (1974) paper.

Gassmann equations

White (1965) formulated the Gassmann model for P-wave velocity v_P as

$$v_P = \left\{ \frac{1}{\rho_b} \left[K_d + \tfrac{4}{3}\mu_d + \frac{\left(1 - \frac{C_m}{C_d}\right)^2}{C_m(1-\phi) + C_f\phi - \frac{C_m^2}{C_d}} \right] \right\}^{1/2}, \tag{A14}$$

where $\rho_b = \rho_m(1-\phi) + \rho_f\phi$, K_d and μ_d are the bulk and shear moduli of the dry rock, and C_m, C_f and C_d are, respectively, the grain matrix (matrix), fluid and dry rock frame compressibilities, given by

$$C_m = \frac{1}{K_m}, \tag{A15}$$

$$C_f = \frac{1}{K_f} \tag{A16}$$

and

$$C_d = \frac{1}{K_d}. \tag{A17}$$

The shear-wave velocity v_S of the rock permeated by non-viscous fluid is simply

$$v_S = \left\{ \frac{\mu_d}{\rho_b} \right\}^{1/2}. \tag{A18}$$

References

Blangy J.P. and Nur A. 1992. A new look at ultrasonic shear velocities in sands. SEG/EAEG summer research workshop, Big Sky, Montana. Expanded Abstracts, 374–376.

Blangy J.P., Strandenes S., Moos D. and Nur A. 1993. Ultrasonic velocities in sands–revisited. *Geophysics* 58, 344–356.

Bruner W.M. 1976. Comment on "Seismic Velocities in Dry and Saturated Cracked Solids" by Richard J. O'Connell and Bernard Budianskey. *Journal of Geophysical Research* 81, 2573–2576.

Castagna J.P., Batzle M.L. and Eastwood R.L. 1985. Relationships between compressional-wave and shear-wave velocities in clastic silicate rocks. *Geophysics* **50**, 571–581.

Cheng C.H. and Toksöz M.N. 1979. Inversion of seismic velocities for pore aspect ratio spectrum of a rock. *Journal of Geophysical Research* **84**, 7533–7543.

Domenico S.N. 1976. Effect of brine–gas mixture on velocity in an unconsolidated reservoir. *Geophysics* **41**, 882–894.

Gassmann F. 1951. Elasticity of porous media. *Vierteljahrschrift der Naturforschenden Gesellschaft in Zürich* **96**, 1–21.

Gist G.A. 1994. Interpretation of laboratory velocity measurements in partially gas-saturated rocks. *Geophysics* **59**, 1100–1109.

Greenberg M.L. and Castagna J.P. 1992. Shear-wave velocity estimation in porous rocks: theoretical formulation, preliminary verification and applications. *Geophysical Prospecting* **40**, 195–209.

Han D., Nur A. and Morgan D. 1986. Effect of porosity and clay content on wave velocity in sandstones. *Geophysics* **51**, 2093–2107.

Hornby B.E., Schwartz L.M. and Hudson J.A. 1994. Anisotropic effective-medium modelling of elastic properties of shales. *Geophysics* **59**, 1570–1583.

Hudson J.A. 1981. Wave speed and attenuation of elastic waves in material containing cracks. *Geophysical Journal of the Royal Astronomical Society* **64**, 133–150.

Klimentos T. 1991. The effects of porosity-permeability-clay content on the velocity of compressional waves. *Geophysics* **56**, 1930–1939.

Klimentos T. and McCann C. 1990. Relationships between compressional wave attenuation, porosity, clay content, and permeability of sandstones. *Geophysics* **55**, 998–1014.

Knight R. and Nolen-Hoeksema R. 1990. A laboratory study of the independence of elastic wave velocities on pore scale fluid distribution. *Geophysical Research Letters* **17**, 1529–1532.

Kuster G.T. and Toksöz M.N. 1974. Velocity and attenuation of seismic waves in two phase media: Part 1: Theoretical formulation. *Geophysics* **39**, 587–606.

Marion D., Nur A., Yin H. and Han D. 1992. Compressional velocity and porosity in sand–clay mixtures. *Geophysics* **57**, 554–563.

Mavko G. and Jizba D. 1991. Estimating grain-scale fluid effects on velocity dispersion in rocks. *Geophysics* **56**, 1940–1949.

Mukerji T. and Mavko G. 1994. Pore fluid effects on seismic velocity in anisotropic rocks. *Geophysics* **59**, 233–244.

Murphy W. 1984. Acoustic measures of partial gas saturations in tight sandstones. *Journal of Geophysical Research* **89**, 11549–11559.

Rafavich F., Kendall C.H.St.C. and Todd T.P. 1984. The relationship between acoustic properties and the petrographic character of carbonate rocks. *Geophysics* **49**, 1622–1636.

Rider M.H. 1991. *The Geological Interpretation of Well Logs*. Whittles Publishing, Caithness.

Serra, O. 1984. *Fundamentals of Well-Log Interpretation. I: The Acquisition of Logging Data*. Elsevier Science Publishing Co.

Tosaya C.A. 1982. *Acoustical properties of clay-bearing rocks*. Ph.D. thesis, Stanford University.

Wang Z. and Nur A. 1992. Elastic wave velocities in porous media: a theoretical recipe. In: *Seismic and Acoustic Velocities in Reservoir Rocks, Vol. 2, Theoretical and Model Studies* (eds Z. Wang and A. Nur), S.E.G., Tulsa, pp. 1–35.

White J.E. 1965. *Seismic Waves: Radiation, Transmission, and Attenuation.* McGraw–Hill Book Co.

Winkler K.W. and Nur A. 1982. Effects of pore fluids and frictional sliding on seismic attenuation. *Geophysics* 47, 1–12.

Wood A.W. 1941. *A Textbook of Sound.* The Macmillan Publishing Company, New York.

Xu S. and White R.E. 1995a. A new velocity model for clay–sand mixtures. *Geophysical Prospecting* 43, 91–118.

Xu S. and White R.E. 1995b. Poro-elasticity of clastic rocks: a unified model. 36th Annual Logging Symposium, Paris, France, Transactions, Paper V.

Xu S. and White R.E. 1995c. Comparison of four schemes for modelling anisotropic P-wave and S-wave velocities in sand–shale systems. 57th EAEG meeting, Glasgow, UK, Expanded Abstracts, Paper B2.

Yin H., Han D.H. and Nur A. 1988. Study of velocities and compaction on sand–clay mixtures. Stanford University, S.R.B. report 33.